Particle Simulation of Plume-Plume and Plume-Surface Interactions

S.F. Gimelshein
Research Assistant Professor
Department of Aerospace and Mechanical Engineering
201 Rapp Research Building, University of Southern California,
Los Angeles, 90089
Tel: 213-740-9211, Fax: 213-740-7774, Email: gimelshe@usc.edu

A.D. Ketsdever
Senior Research Engineer
AFRL/PRSA, 10 E. Saturn Blvd, Edwards AFB, CA 93524-7680
Tel: 661-275-6242, Email: Andrew.Ketsdever@edwards.af.mil

D.C. Wadsworth
Scientist
ERC, Incorporated, 10 E. Saturn Blvd., Edwards AFB, CA 93524
Tel: 661-275-5153; Email: Dean.Wadsworth@edwards.af.mil

Numerical modeling of two- and three-dimensional low Reynolds number gas flows from small nozzles has been performed using the direct simulation (DSMC) method. The objective of this effort is to gain an improved understanding of performance and plume interaction phenomena for low thrust devices, and thus improve the design and optimization process for a variety of micro-propulsion systems. Simulations were performed for a wide range of flow parameters using the SMILE parallel DSMC code. Validation has been conducted through comparison of mass flow and thrust values obtained numerically with results of experimental measurements carried out recently by AFRL researchers. Good agreement observed between simulation and experiment provided credibility to important findings related to plume-plume and plume-surface interactions. In particular, a large effect of plume interaction on surface back force and net nozzle thrust has been shown for low Reynolds flows. The influence of the gas surface interaction accommodation coefficient on nozzle performance was also investigated. An example of the plume flow from a 4cm diameter nozzle interacting with a plate is shown in Figs. 1 and 2 where the pressure field and surface pressure distribution are shown for a throat Reynolds number of 60 and nitrogen propellant.

HPC resources used: up to 64 processors of Linux cluster huinalu (MHPCC).
Other resources used: 28 processors of a USC PC Linux cluster.

Publications:

A. Ketsdever, N. Selden, S. Gimelshein, A. Alexeenko, P. Vashchenkov and M. Ivanov, Plume Interactions of Multiple Jets Expanding into Vacuum: Experimental and Numerical Investigation, AIAA Paper 2004-1248.

A. Ketsdever, M. Clabough, S. Gimelshein, A. Alexeenko Experimental and Numerical Determination of Micropropulsion Device Efficiencies at Low Reynolds Numbers, Submitted to AIAA Journal.

Acknowledgement:
This work was performed under DoD HPCMP project 0468, Nonequilibrium Flow Modeling.

Report Documentation Page

Form Approved
OMB No. 0704-0188

1. REPORT DATE	2. REPORT TYPE	3. DATES COVERED
SEP 2004		**-**

4. TITLE AND SUBTITLE	5a. CONTRACT NUMBER
Particle Simulation of Plume-Plume and Plume-Surface Interactions	5b. GRANT NUMBER
	5c. PROGRAM ELEMENT NUMBER
6. AUTHOR(S)	5d. PROJECT NUMBER
S. Gimelshein; A. Ketsdever; D. Wadsworth	**2308**
	5e. TASK NUMBER **M19B**
	5f. WORK UNIT NUMBER
7. PERFORMING ORGANIZATION NAME(S) AND ADDRESS(ES)	8. PERFORMING ORGANIZATION REPORT NUMBER
Air Force Research Laboratory (AFMC),AFRL/PRSA,10 E. Saturn Blvd.,Edwards AFB,CA,93524-7680	
9. SPONSORING/MONITORING AGENCY NAME(S) AND ADDRESS(ES)	10. SPONSOR/MONITOR'S ACRONYM(S)
	11. SPONSOR/MONITOR'S REPORT NUMBER(S)

12. DISTRIBUTION/AVAILABILITY STATEMENT

Approved for public release; distribution unlimited

13. SUPPLEMENTARY NOTES

14. ABSTRACT

Numerical modeling of two- and three-dimensional low Reynolds number gas flows from small nozzles has been performed using the direct simulation (DSMC) method. The objective of this effort is to gain an improved understanding of performance and plume interaction phenomena for low thrust devices and thus improve the design and optimization process for a variety of micro-propulsion systems. Simulations were performed for a wide range of flow parameters using the SMILE parallel DSMC code. Validation has been conducted through comparison of mass flow and thrust values obtained numerically with results of experimental measurements carried out recently by AFRL researchers.

15. SUBJECT TERMS

16. SECURITY CLASSIFICATION OF:			17. LIMITATION OF ABSTRACT	18. NUMBER OF PAGES	19a. NAME OF RESPONSIBLE PERSON
a. REPORT	b. ABSTRACT	c. THIS PAGE			
unclassified	**unclassified**	**unclassified**		**6**	

Figure Captions:
Figure 1. Interaction of nozzle plume with offset horizontal plate (flowfield pressure contours on plume symmetry plane).
Figure 2. Enhancement of plume backflow due to presence of plate (oblique view of surface pressure contours on nozzle, horizontal plate and nozzle backplate).

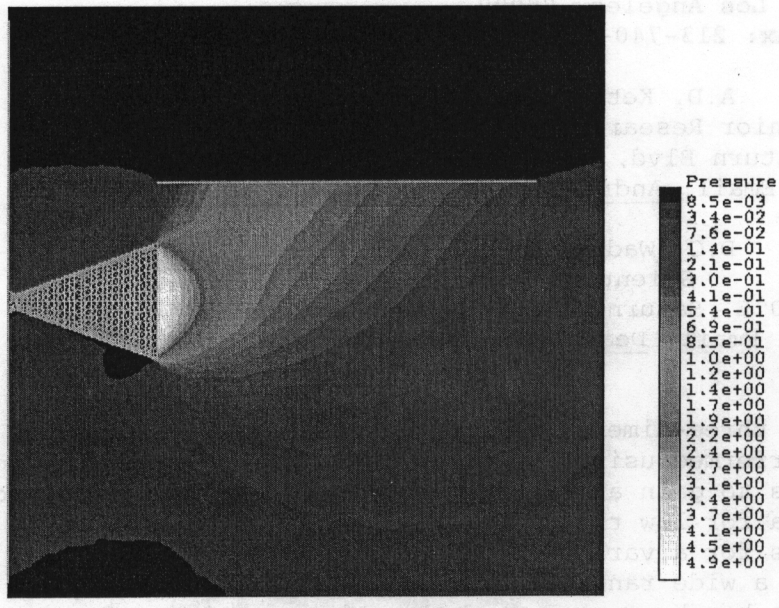

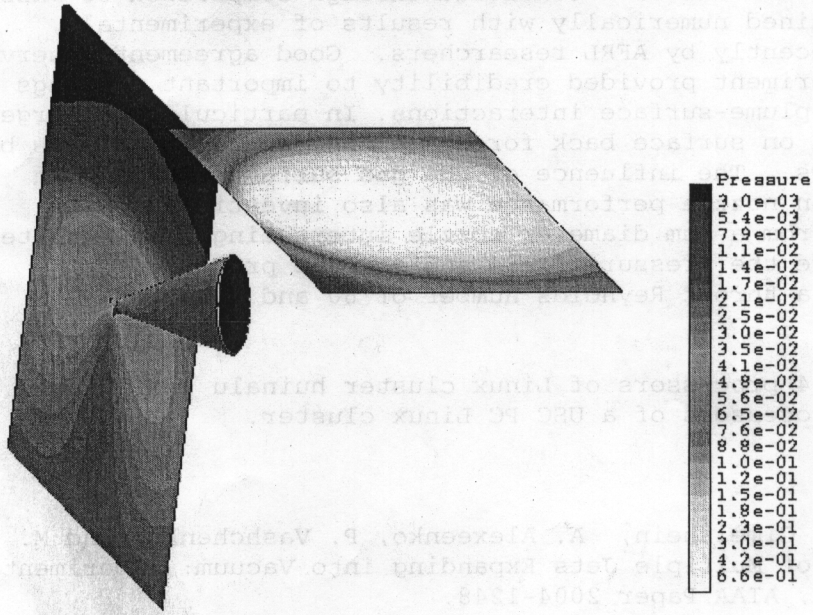

Here R_p is the particle radius, n_g is the gas number density, $f(\mathbf{u}_r)$ is the gas velocity distribution function in a particle-centered coordinate frame, m is the mass per gas molecule, c_r is the relative speed, τ is the particle thermal accommodation coefficient, T_p is the particle temperature and k_B is Boltzmann's constant.

In considering the Green's function $\mathbf{F}_p(\mathbf{u}_r)$ for the force imparted by the gas on a rotating particle, we first decompose $\mathbf{F}_p$ into a term which accounts for momentum transfer to the particle from incident gas molecules, a term for momentum exchange during specular reflection, and a corresponding term for diffuse reflection. It can be shown that the second term is zero and that only the third term may be influenced by particle rotation. Next, using the velocity superposition principle, the momentum transfer due to diffuse reflection is separated into a component independent of rotation and a component which depends on the particle angular velocity ω_p but is independent of T_p. This latter component is the only contributor in a time-averaged sense to the force Green's function $\mathbf{F}_{rot}$ due to particle rotation, and allows the Green's function for the total force on the particle to be computed as $\mathbf{F}_p = \mathbf{F}_{nr} + \mathbf{F}_{rot}$. Following the above logic, $\mathbf{F}_{rot}$ is equal to the product of the collision frequency for diffusely reflecting collisions and the rotational component $-m\langle\mathbf{u}_t\rangle$ of the average momentum transferred to the particle during diffuse reflection. Here $\mathbf{u}_t$ is the tangential velocity of the particle surface at the collision point in an inertial particle-centered reference frame. In order to evaluate $\langle\mathbf{u}_t\rangle$ we express $\mathbf{u}_t$ as a function of the angle θ between $-\mathbf{u}_r$ and the outward surface normal unit vector $\mathbf{n}_c$ at the collision point, then multiply by the distribution function for θ and integrate over all particle surface elements where a collision may occur. We find:

$$\mathbf{F}_{rot}(\mathbf{u}_r) = \frac{2\pi}{3} R_p^3 m n_g f(\mathbf{u}_r) \tau \, \boldsymbol{\omega}_p \times \mathbf{u}_r \tag{2}$$

By adding (1) and (2) and integrating over all gas velocity space, we then determine the total force on the particle.

In the absence of any gas vorticity effects or forces not associated with interphase collisions, the rotating particle will experience a damping moment about the particle center which will tend over time to reduce the magnitude of ω_p. Depending on the angle between ω_p and the gas bulk velocity relative to the particle, the moment may also have a component orthogonal to ω_p which tends to change the axis about which the particle rotates. This moment can be determined using the same Green's function approach as above. Again, incident and specularly reflected gas molecules do not contribute to the moment, and the average moment contribution during diffuse reflection depends only on the tangential velocity of the particle surface. The Green's function $\mathbf{M}_p(\mathbf{u}_r)$ for this moment can then be expressed as the negative product of the collision frequency for diffuse reflection and the average angular momentum $mR_p\langle\mathbf{n}_c \times \mathbf{u}_t\rangle$ about the particle center imparted on diffusely reflected gas molecules. The averaging operation is performed through integration over the particle surface, to find the following result:

$$\mathbf{M}_p(\mathbf{u}_r) = \frac{1}{4} \pi R_p^4 m n_g f(\mathbf{u}_r) \tau c_r \left(\frac{\mathbf{u}_r \cdot \boldsymbol{\omega}_p}{c_r^2} \mathbf{u}_r - 3 \boldsymbol{\omega}_p \right) \tag{3}$$

Through energy conservation arguments, the Green's function for the heat transfer rate to a rotating particle can be expressed as

$$\dot{Q}_p(\mathbf{u}_r) = \pi R_p^2 n_g f(\mathbf{u}_r) \tau c_r \left[\frac{1}{2} m c_r^2 - e_{kin} + \left(e_{rot} - \frac{1}{2} \Lambda_{rot} k_B T_p \right) \right] - \mathbf{M}_p(\mathbf{u}_r) \cdot \boldsymbol{\omega}_p \tag{4}$$

where e_{rot} is the average rotational energy of incident gas molecules, Λ_{rot} is the number of rotational degrees of freedom for the gas, and $e_{kin} = 2k_B T_p + \frac{1}{2} m \langle \mathbf{u}_t \cdot \mathbf{u}_t \rangle$ is the average kinetic energy of diffusely reflected gas molecules in an inertial particle-fixed coordinate frame. By integrating over the particle surface, we derive the general formula

$$\dot{Q}_p(\mathbf{u}_r) = \pi R_p^2 n_g f(\mathbf{u}_r) \tau c_r \left[\frac{1}{2} m c_r^2 - \left(2 + \frac{1}{2} \Lambda_{rot} \right) k_B T_p + e_{rot} + \frac{1}{8} m a_p^2 R_p^2 \left(3 - \frac{(\mathbf{u}_r \cdot \boldsymbol{\omega}_p)^2}{c_r^2 a_p^2} \right) \right] \tag{5}$$

where $a_p = |\boldsymbol{\omega}_p|$. Note from (5) that a greater value of a_p corresponds to an increase in heat transfer from the gas to the particle. This property can be justified physically by considering a single particle surface element in a coordinate frame which is fixed to the local tangential surface velocity. In this coordinate frame the average kinetic energy of diffusely reflected gas molecules will be independent of a_p, while the average kinetic energy of incident gas molecules tends to increase as a_p^2. Thus, the only effect of particle rotation here is to increase the interphase energy transfer associated with the kinetic energy of incident gas molecules which are involved in diffusely reflecting collisions.

In the special case where the particle which moves at the bulk velocity of an equilibrium simple gas with temperature T_g, (5) may be integrated analytically over all gas velocity space to provide a closed form solution for the net heat transfer rate:

$$\dot{Q}_{p,\,rot} = R_p^2\, n_g\, \tau \sqrt{2\pi k_B T_g / m}\left[\left(4+\Lambda_{rot}\right)k_B\left(T_g - T_p\right)+\frac{2}{3}m\alpha_p^2 R_p^2\right] \tag{6}$$

If $T_p > T_g$ as is typical for high-altitude rocket exhaust plume flows, then the two bracketed terms in (6) are of opposite sign. Assuming the first term is greater in magnitude than the second, we find that particle rotation tends to reduce the magnitude of the heat transfer rate and allows for a more gradual reduction in T_p over time.

DSMC IMPLEMENTATION

The Green's functions given above can be used to allow rotating solid particles to be modeled within a DSMC simulation. For simplicity we neglect radiative heat transfer and assume the particle phase to be dilute and chemically inert, so that temporal variation in the properties of individual particles may occur only through the mechanisms described above or through particle-wall interactions. Representative solid particles are tracked along with DSMC gas molecules through a computational grid, and during each time step the total force, moment, and heat transfer rate for each particle is determined by adding contributions from all gas molecules which are assigned to the same cell. The force, moment and heat transfer contributions to a particle from a single DSMC gas molecule are computed by evaluating (1), (2), (3) and (5) with the quantity $n_g f(\mathbf{u}_r)$ replaced by the ratio of the local gas molecule weighting factor to the cell volume. Once all N_g molecules in the cell have been considered, the particle velocity $\mathbf{u}_p$ and temperature T_p are altered as described in Ref. [8], and ω_p is updated by the product of the net moment, the local time step and the inverse of the particle moment of inertia.

Due to the large particle phase mass fractions typical of the high-altitude plume flows of interest, accurate simulation requires consideration of momentum and energy coupling from the particles to the gas. This is accomplished here by probabilistically modeling individual interphase collisions and modifying the velocity and rotational energy of all gas molecules involved. A collision selection scheme based on the No Time Counter method of Bird [12] is used to determine which, if any, DSMC gas molecules will collide with each solid particle during a given time step. If a particular gas molecule is found to collide with the particle, then the collision will involve either diffuse reflection, with probability τ, or specular reflection, with probability $1-\tau$. In the latter case, the post-collision relative velocity $\mathbf{u}_r^*$ is sampled from an isotropic distribution such that the relative speed c_r of the molecule is unchanged during the collision, and the molecule velocity is reassigned to equal $\mathbf{u}_p+\mathbf{u}_r^*$. In the case of diffuse reflection, a more complicated procedure is required to find $\mathbf{u}_r^*$, and the gas molecule rotational energy must be altered as well.

If a gas molecule is diffusely reflected off a nonrotating solid particle, then the magnitude and direction of $\mathbf{u}_r^*$ are statistically independent, so each can be determined separately. Following the procedure outlined in Ref. [8], the post-collision relative speed c_r^* is sampled from the distribution function

$$f(c_r^*)dc_r^* = 2\beta_p^4 c_r^{*3}\exp(-\beta_p^2 c_r^{*2})dc_r^* \tag{7}$$

using the acceptance-rejection method [12], where $\beta_p = \sqrt{m/(2k_B T_p)}$. The angle δ between the vectors $-\mathbf{u}_r$ and $\mathbf{u}_r^*$ is also determined using the acceptance-rejection method, by sampling from a numerical approximation

$$f(\delta) = 0.02042\delta^6 - 0.2515\delta^5 + 1.104\delta^4 - 1.903\delta^3 + 0.4938\delta^2 + 1.248\delta \tag{8}$$

of the distribution function for $\delta \in [0, \pi]$. An azimuthal angle α_0 required to define the direction of $\mathbf{u}_r^*$ in three dimensional space is sampled from a uniform distribution over $[0, 2\pi]$, and the components of $\mathbf{u}_r^*$ are calculated using formulas derived by Bird [12] for binary elastic collisions:

$$u_r^* = \frac{c_r^*}{c_r}\left[-u_r\cos\delta + \sin\delta\sin\alpha_0\left(v_r^2+w_r^2\right)^{1/2}\right],\quad v_r^* = \frac{c_r^*}{c_r}\left[-v_r\cos\delta - \frac{\sin\delta\left(c_r w_r\cos\alpha_0 + u_r v_r\sin\alpha_0\right)}{\left(v_r^2+w_r^2\right)^{1/2}}\right],\quad w_r^* = \frac{c_r^*}{c_r}\left[-w_r\cos\delta + \frac{\sin\delta\left(c_r v_r\cos\alpha_0 - u_r w_r\sin\alpha_0\right)}{\left(v_r^2+w_r^2\right)^{1/2}}\right] \tag{9}$$

The absolute velocity of the gas molecule is then set to the final value $\mathbf{u}_p+\mathbf{u}_r^*$.

If a diffusely reflecting collision involves a rotating solid particle, then Eq. 8 is not valid and an alternate procedure must be used. In this case $\mathbf{u}_r^*$ is found by separately determining nonrotational $\mathbf{u}_{nr}^*$ and rotational $\mathbf{u}_{rot}^*$ components, then adding the two together. To calculate $\mathbf{u}_{nr}^*$, we first compute the angle θ between $-\mathbf{u}_r$ and the outward normal unit vector $\mathbf{n}_c$ at the collision point on the particle surface by setting $\sin^2\theta$ equal to a random number on $[0, 1]$. A corresponding azimuthal angle α_1 is sampled from a uniform distribution over $[0, 2\pi]$, and components of $\mathbf{n}_c$ are then calculated as

$$n_{c,x} = \frac{1}{c_r}\left[-u_r\cos\theta + \sin\theta\sin\alpha_1\left(v_r^2+w_r^2\right)^{1/2}\right],\quad n_{c,y} = \frac{1}{c_r}\left[-v_r\cos\theta - \frac{\sin\theta\left(c_r w_r\cos\alpha_1 + u_r v_r\sin\alpha_1\right)}{\left(v_r^2+w_r^2\right)^{1/2}}\right],\quad n_{c,z} = \frac{1}{c_r}\left[-w_r\cos\theta + \frac{\sin\theta\left(c_r v_r\cos\alpha_1 - u_r w_r\sin\alpha_1\right)}{\left(v_r^2+w_r^2\right)^{1/2}}\right] \tag{10}$$

Next, we find the angle ζ between the vectors $\mathbf{n}_c$ and $\mathbf{u}_{nr}^*$ by sampling $\sin^2\zeta$ from a uniform distribution over [0, 1]. An azimuthal angle α_2 is sampled from a uniform distribution over [0, 2π], and Eq. 7 is used to find the magnitude of $\mathbf{u}_{nr}^*$. The components of $\mathbf{u}_{nr}^*$ are then determined through the following equations:

$$u_{nr}^* = c_r^* \left[n_{c,x}\cos\zeta + \sin\zeta \sin\alpha_2 (1-n_{c,x}^2)^{1/2} \right],\ v_{nr}^* = c_r^* \left[n_{c,y}\cos\zeta + \frac{\sin\zeta (n_{c,z}\cos\alpha_2 - n_{c,x}n_{c,y}\sin\alpha_2)}{(1-n_{c,x}^2)^{1/2}} \right],\ w_{nr}^* = c_r^* \left[n_{c,z}\cos\zeta - \frac{\sin\zeta (n_{c,y}\cos\alpha_2 + n_{c,x}n_{c,z}\sin\alpha_2)}{(1-n_{c,x}^2)^{1/2}} \right] \quad (11)$$

Finally, the rotational component of $\mathbf{u}_r^*$ is computed as $\mathbf{u}_{rot}^* = R_p\,\omega_p \times \mathbf{n}_c$, and the gas molecule velocity is reassigned to the post-collision value $\mathbf{u}_p + \mathbf{u}_{nr}^* + \mathbf{u}_{rot}^*$.

PLUME SIMULATION

To evaluate the importance of particle rotation effects, all procedures described above are implemented in the DSMC code MONACO [10], and an axisymmetric simulation is performed for the nearfield plume flow from a Star-27 solid rocket motor expelling into a vacuum. The nozzle has an exit diameter of 78 cm and a divergence half-angle of 17.2°. All gas and particle properties along the nozzle exit plane are taken from Anfimov et al. [11] Based on values provided by these authors, spherical Al_2O_3 particles of diameter D_p = 0.15, 0.2, 0.3, 0.5, 1, 2 and 3 μm together constitute a total mass flow fraction of about 30%, with particles of each size distributed uniformly over the nozzle exit. The gas here is a mixture of H_2, N_2 and CO, with mole fractions of 0.38, 0.31, and 0.31 respectively. Effects of radiative heat transfer, heterogeneous reactions, gas chemistry and particle phase change are neglected. While each of these phenomena may significantly alter flow properties of interest, we intend only to assess the importance of particle rotation effects on a representative plume flow, not to calculate flow properties for a particular case with the greatest possible accuracy.

Following Vasenin et al. [2], we assume that coalescing collisions between liquid droplets within the nozzle are the dominant contributors to particle rotation. The maximum allowable particle angular velocity magnitude is then determined by a criterion for the centrifugal breakup of liquid droplets. A normalized angular velocity

$$\Omega = \frac{4}{5}\,\omega_p \sqrt{\frac{\pi}{3}\frac{m_p}{\sigma}} \quad (12)$$

is set to equal some critical value Ω_{crit} for all particles at the nozzle exit, where m_p is the particle mass and σ is the liquid surface tension of the particle material. While the magnitude of ω_p will be constant for all particles of equal diameter at the nozzle exit, the initial direction of ω_p for each particle is randomly selected on a plane normal to the axis of symmetry. Salita [1] uses momentum and energy conservation arguments to show that the collision-induced rotation rate of spherical liquid agglomerates should be limited by Ω_{crit}=3.31. Following these arguments, we perform plume simulations with initial particle angular velocities corresponding to Ω=3.31 and Ω=0 in order to evaluate potential upper bounds for the influence of particle rotation on various flow properties. For both cases, particle-to-gas coupling is considered through application of the method described above involving (10) and (11), to avoid any differences in results caused by the numerical approximation in (8).

The simulations use a rectangular grid domain, starting at the nozzle exit plane and extending 10 m downstream in the axial direction and 4 m in the radial direction. Calculations are performed on 16 1.4 GHz AMD Opteron processors, with each case requiring about 3000 CPU hours. As an example of simulation results for the Ω=3.31 case, Figure 1 shows average angular velocity magnitudes for particles of each size as a function of distance from the central axis, along a radial plane 10 m downstream of the nozzle exit. Figure 2 shows the variation in average particle temperatures along this same plane, for both the Ω=3.31 and Ω=0 cases. From a comparison of T_P values for any radial location and particle size, particle rotation is shown in Figure 2 to have little measurable impact on particle temperatures in the plume. However, for all but the largest and smallest particles considered, rotation does account for a roughly 5 to 10 K increase in average particle temperatures within about 0.5 m of the central axis. This trend is likely due to the fact that the gas density, and therefore the component of the interphase energy transfer rate associated with particle rotation, tends to decrease with distance from the axis. The trend is less pronounced for the smallest particles because these rapidly lose the bulk of their rotational energy on entering the grid domain, and for the largest particles because of their relatively low initial angular velocities.

With this one minor exception, we find a general lack of dependence on particle rotation for all flow properties of interest. Distributions of gas translational temperature, particle and gas number densities, maximum divergence angles for each particle size, and various other properties show differences between the two cases which are comparable to the expected statistical scatter. We can therefore conclude that, at least for the plume simulation

considered here, particle rotation may be neglected with no significant loss in overall accuracy. The numerical methods described above do maintain some utility in making this conclusion possible, and in allowing for the simulation of other two-phase rarefied flows, such as MEMS flows involving frequent particle-wall collisions, where rotation effects may still be important.

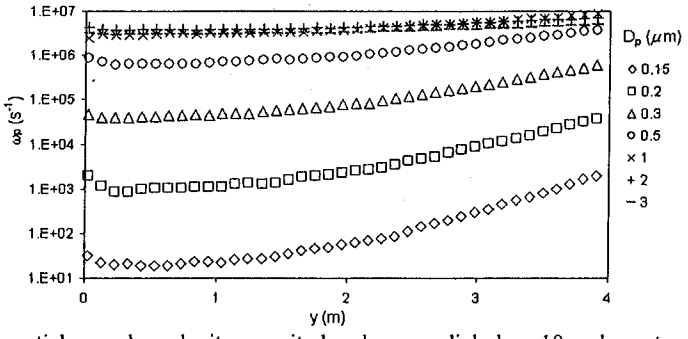

FIGURE 1. Variation in particle angular velocity magnitudes along a radial plane 10 m downstream from the nozzle exit.

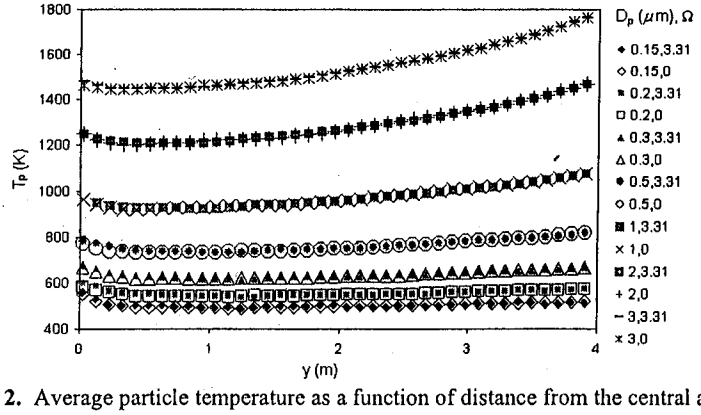

FIGURE 2. Average particle temperature as a function of distance from the central axis.

ACKNOWLEDGMENTS

The authors gratefully acknowledge financial support for this work from the Air Force Research Laboratory at Edwards Air Force Base, with Dean Wadsworth and Tom Smith as technical monitors.

REFERENCES

1. Salita, M., J. Propulsion and Power 7, 505-512 (1991).
2. Vasenin, I. M., Narimanov, R. K., Glazunov, A. A., Kuvshinov, N. E., and Ivanov, V. A., J. Propulsion and Power 11, 583-592 (1995).
3. Crowe, C., Sommerfeld, M., and Tsuji, Y., Multiphase Flows with Droplets and Particles, CRC, New York, 1998, p. 99.
4. Simmons, F. S., Rocket Exhaust Plume Phenomenology, Aerospace Press, El Segundo, CA, 2000, pp.21-30.
5. Epstein, P. S., Phys. Review 24, 710-732 (1924).
6. Wang, C., AIAA Journal 10, 713-714 (1972).
7. Ivanov, S. G., and Yanshin, A. M., Fluid Dynamics 15, 449-453 (1980).
8. Burt, J. M., and Boyd, I. D., AIAA Paper 2004-1351 (2004).
9. Gallis, M. A., Torczynski, J. R., and Rader, D. J., Physics of Fluids 13, 3482-3492 (2001).
10. Dietrich, S., and Boyd, I. D., J. Computational Physics 126, 328-342 (1996).
11. Anfimov, N. A., Karabadjak, G. F., Khmelinin, B. A., Plastinin, Y. A., and Rodionov, A. V., AIAA Paper 93-2818 (1993).
12. Bird, G. A., Molecular Gas Dynamics and the Direct Simulation of Gas Flows, Clarendon Press, Oxford, 1994, pp. 34-36, 218-220, 425.